Mechanical properties of viscoelastic materials subjected to thermal-oxidative aging: an experimental and theoretical study

Mechanical properties of viscoelastic materials subjected to thermal-oxidative aging: an experimental and theoretical study

Qiang-Qiang Li[1], Zhao-Dong Xu[1*], Quek-Ser Tong[2], Yao-Rong Dong[3], Ye-Shou Xu[1], Yong Lu[4]

[1] *China-Pakistan Belt and Road Joint Laboratory on Smart Disaster Prevention of Major Infrastructures, Southeast University, Nanjing 211189, China;*

[2] *Department of Civil and Environmental Engineering, National University of Singapore, Singapore 117576, Singapore*

[3] *School of Civil Engineering, Xi'an University of Architecture and Technology, Xi'an 710055, China;*

[4] *Institute for Infrastructure and Environment, School of Engineering, The University of Edinburgh, Edinburgh EH9 3JL, United Kingdom*

Correspondence: zhdxu@163.com

Abstract: Viscoelastic materials (VEMs) made from rubber polymer will inevitably age due to the interactions with the harmful environment during service life, thus reducing the reliability of viscoelastic (VE) damping equipment installed in building structures. In order to understand and be able to predict the degradation of VE damping equipment, it is imperative to comprehensively study the influence of aging on the mechanical properties of VEMs. In this paper, a series of thermal-oxidative (TO) aging tests and mechanical property tests are conducted on our previously developed VEMs to study effects of TO aging on the molecular chain structure and corresponding changes of macroscopic mechanical properties of VEMs. By classifying molecular chains of VEMS into elastic chains and free chains, the effects of different chemical reactions during TO aging on these two main chains and corresponding changes on macroscopic mechanical behaviors of VEMs are analyzed. This facilitates formulating a mathematical model that can characterize the mechanical behavior of TO aging VEMs. In conjunction with the experimental data, the accuracy and applicability of the proposed model are compared and verified. Sensitivity analyses of parameters involved in the proposed model are then performed. The experimental results demonstrate that the TO aging can degrade the deformation capability and harden the modulus of VEMs, which may adversely affect the performance

of VE damping devices. The parameter analyses depict that the TO aging affects the macroscopic mechanical behavior of VEMs by altering the relative number and configuration of free chains and elastic chains as well as their respective contributions to the total stress of VEMs. The results point to the high accuracy of the proposed model in representing the strain-stress behavior of VEMs under different aging conditions.

Keywords: viscoelastic material; thermal-oxidative aging; mechanical property test; molecular chain structure; microscopic model.

1 Introduction

Due to the unique physical-mechanical properties, such as large recoverable deformation, excellent dielectric properties, good air tightness, strong processability, rubber polymer has become a preferred engineering material, which is widely used in precision instruments, aerospace, industrial equipment, biomedicine, and other fields with satisfactory results [1, 2].

In recent decades, with the development of design concept in energy dissipation and vibration mitigation of civil engineering structures, many researchers have attempted to introduce rubber polymer materials into the field of structural vibration control. For example, our research group developed a series of high-dissipation viscoelastic materials (VEMs) based on different rubber matrixes [3, 4], and use them in viscoelastic (VE) devices for building to experimentally and theoretically study their dynamic mechanical properties [5-7]. At the structural level, many scholars [8-11] conducted numerous experiments on various VE equipment developed for different civil

engineering structures, and concluded that these VE devices could significantly reduce the responses of structures under dynamic loadings, thus effectively protecting the entire structural system.

Generally, the service life of civil engineering structures spans at least several decades under complex working environments, thus VEMs are inevitably subjected to a series of physical-chemical reactions due to the invasion of external harmful agents, causing adverse aging [12]. Consequently, the performance of VEMs degrades, resulting in poor isolation and damping effect of VE equipment, which finally leads to unpredictable risks in the safety of structures [13]. This means that it is imperative to study the effect of aging on the mechanical properties of VEMs, especially when there are few published reports on the aging of VEMs used in civil engineering.

Depending on the operating environment, VEMs may have varying physical-chemical reactions with different media and thus undergo different types of aging and exhibit different aging consequences [14, 15]. Considering the high percentage of oxygen in the atmosphere, TO aging is one of the most common aging types for rubber polymer [15, 16], and hence may be the predominant type of aging experienced by VE equipment.

There are many studies on TO aging of rubber polymers. Experimentally, various researchers [12, 13, 17-20] studied the changes in mechanical behaviors of rubber polymers before and after aging and interpreted the mechanism of TO aging on material properties from the molecular-chain level. Theoretically, phenomenological models have been employed [21-27] to describe the mechanical behavior of rubber polymers and introduced the Arrhenius equations to characterize the influence of TO aging, resulting in the formulation of the constitutive behavior of TO aging rubber polymers.

However, due to the phenomenological nature, these models and the model parameters cannot directly reflect the relationship between the physical chain structure of polymer materials and their macroscopic mechanical behaviors. In the process of TO aging, a variety of physical-chemical reactions may occur in rubber polymer under the catalysis of oxygen and heat, which can irreversibly alter the original chain structure of material, leading finally to the performance degradation. As such, the macroscopic aging models may limit the further development in the performance of VEMs.

To reflect the relationship between chain structure and macroscopic mechanical behavior of rubber polymers during TO aging, the chain statistical mechanics has been employed. For example, many scholar [14, 15, 28, 29] analyzed the multiple chemical reactions and chain structure evolution in the rubber polymer during aging, and proposed various chain models by superimposing several microspheres models which is based on free chain assumption. Thus, the introduction of microsphere model to describe the mechanical behavior of rubber polymers has greatly enhanced the link between the theoretical model and actual mechanical behavior as well as giving physical meanings to model parameters.

There are different kinds of molecular chains in rubber polymer, and each type of chain has a special contribution to its macroscopic mechanical properties [30]. The above chain models only give approximate statistics on molecular chains and neglect the differences between chains. They do not consider the effects of different physical-chemical reactions on different types of chains and the corresponding changes on the macroscopic mechanical behavior of material during aging. Thus, researchers cannot clearly comprehend changes of different molecular chains in rubber polymer, and their varied contributions to the total mechanical behavior during the aging process. This restricts the

usefulness of these models in guiding the enhancement and modification of rubber polymer under TO aging conditions in the further development.

In addition, to improve applications of rubber polymers better in civil engineering, different fillers are often added as reinforcement. The physical properties of filled rubber polymer significantly distinct from those of unfilled systems [31-33], and are not considered in the chain models. Moreover, the filler particles are randomly distributed in the rubber matrix [34, 35], and together with the difference in stiffness between the filler particles and rubber matrix will cause deformation that is hard to predict consistently. However, in the above aging chain models, the heterogeneous deformation behavior is often simplified to affine deformation, which is obviously inappropriate.

In this paper, a series of TO aging tests and mechanical property tests are carried out on our previously developed VEMs [4] used for building vibration control to investigate the effects of TO aging on the chain structure and changes on the macroscopic mechanical properties of VEMs. By categorizing the molecular chains of VEMs into two main kinds, the effects of their relative quantities and different reactions due to their structures on the macroscopic behaviors of material are analyzed. A mathematical model for describing the mechanical behavior of TO aging VEMs is then developed by combining the statistical model of molecular chains and the theory of chemical kinetics. Finally, based on the test data, the accuracy and applicability of the proposed model are verified, and the sensitivity of the parameters is analyzed.

2 Mechanical performance tests of thermal-oxidative aging VEMs

2.1 Experimental protocol

The viscoelastic materials studied in this manuscript are based on the Nitrile Butadiene Rubber (N220S, Japan Synthetic Rubber, Japan) matrix, and mixed with organic small molecules (hindered phenol, AO80) and various additives (including zinc oxide, stearic acid, carbon black, accelerating agent, antioxidant, and sulfur) [4]. This study focuses on the influence of TO aging on the mechanical properties of VEMs, and is limited to homogeneous aging rather than heterogeneous aging. According to [36, 37], one can ensure that materials stay in a homogeneous aging state when the thickness of material specimen does not exceed 2 mm. Therefore, a batch of VEMs test pieces with a thickness of 2 mm are prepared and placed in a customized intelligent chamber for aging. To prevent heterogeneous aging of VEMs caused by poor air flow inside chamber, each test piece is suspended and fixed, with a specific distance set between adjacent test pieces. The test temperature (T) is set at 90 ºC, within the range of 80 ºC~120 ºC used in aging test by others [2, 12, 17, 18, 21, 37]. The Figure 1 shows the aging test equipment and a sample specimen.

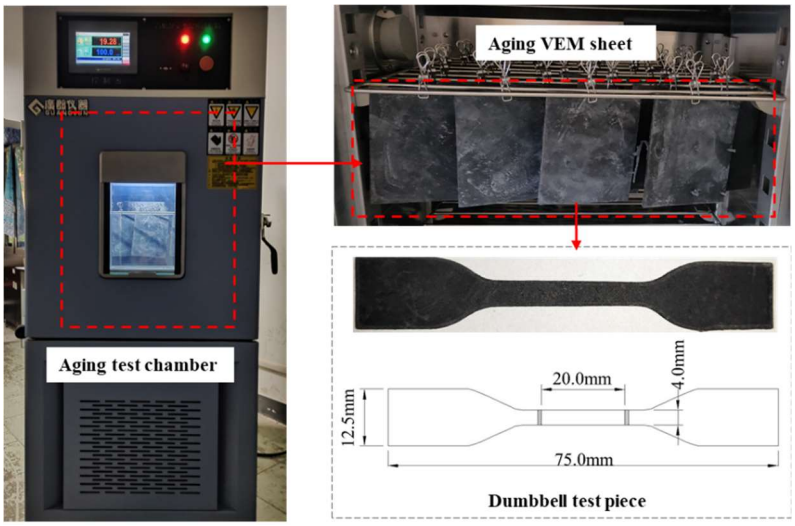

Figure 1 Accelerated aging tests of VEMs

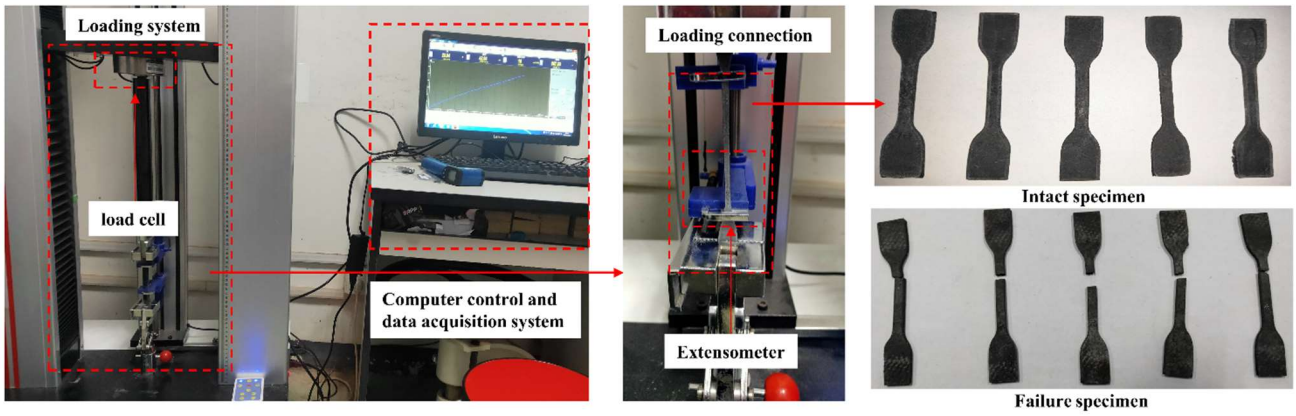

Figure 2 Mechanical property tests of thermal-oxidative aging VEMs

After aging, the mechanical property of aged VEMs were tested by cutting dumbbell shaped samples based on the current code (GB T 528-2009) from the aged VEMs sheets. The setup and specimens are shown in Figure 2. To minimize the effect of variability and measurement error, the mean of five specimens were used for each test conditions (aging time, denoted t_1, in Table 1). Based on the literature [2, 18, 37, 38], the parameter setting of tests are given in Table 1.

Table 1 Parameter setting of aging test and mechanical property test

Aging time (h)	Loading rate (mm/min)	Mech. test temperature (ºC)
0, 20, 80, 160, 240, 320, 480, 640	500	13

2.2 Analysis of test results and aging mechanism

As illustrated in Figure 3, the initial modulus increases with t_1 in both groups, whereas the modulus decreases as the strain increases under each aging time, which is plotted in Figure 4. The rate of stress decrease or modulus degradation is fastest at the beginning (where the strain is small <1.0) and then flattens before increasing again (for strain > 2.0). For the unaged VEMs, the modulus is 2.52 MPa at a strain of 0.60, and changes to 1.81 MPa with strain increasing to 1.80, and it further reduces to 1.54 MPa when strain is 3.00. This phenomenon is mainly because of the accumulated damage in the VEMs during loading. At small strains, chains in the network start to straighten especially those along the

load path, which explains the higher modulus decrease at the beginning. When more chains have straightened, higher stress increase is needed to produce the strain increment which explain the lower rate of modulus change until most chains along the load path have straightened leading to the lowest modulus change (approximate for strains between 1.0 and 2.0). As load increases, the stresses in the straight chains in the network increases to a level when the stress exceeds the bond force especially at the cross-linking points on the short-length chains which may be preferentially destroyed. The short chains are then transformed into a chain with longer effective length, effectively reducing the entropic elasticity of the original short chain. When more and more short chains are transformed into long chains by losing crosslinking points, the whole chain structure will exhibit the phenomenon of reduced entropic elasticity and poor stress transferability, which is the main damage mechanism of VEMs during deformation.

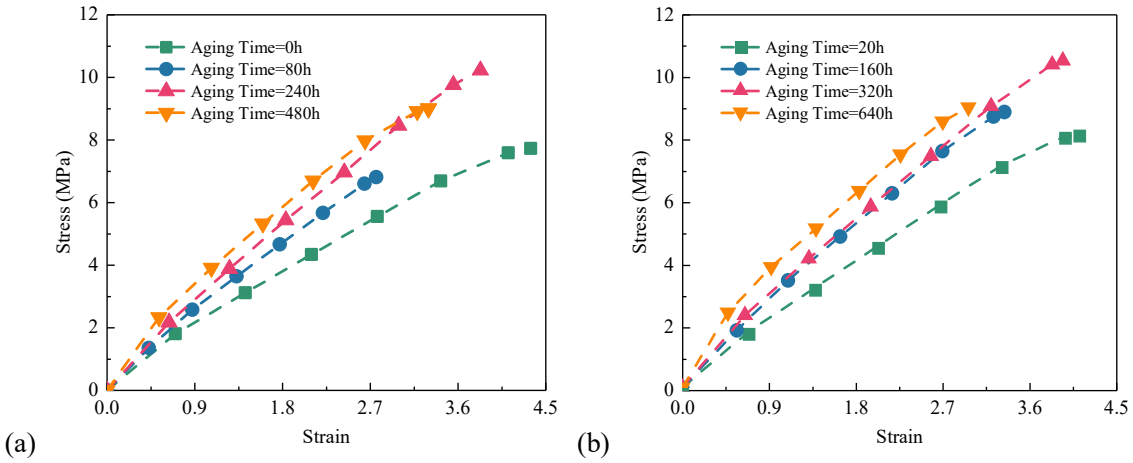

Figure 3 Stress-strain curves of aging VEMs: (a) Group 1: t_1= 0h, 80h, 240h, 480h (b) Group 2: t_1=20h, 160h, 320h, 640h

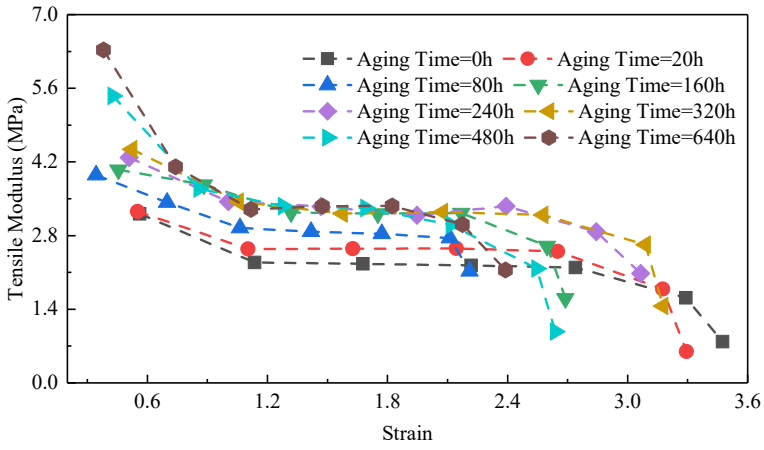

Figure 4 Modulus of VEMs vs. strain under different aging time

The fracture strain (ε_f), fracture stress (σ_f), stress at 100% strain ($\sigma_{100\%}$), and stress at 250% strain ($\sigma_{250\%}$) under different aging times are plotted in Figure 5, and their means, mean squared errors (MSEs), and variances are listed in Table 2.

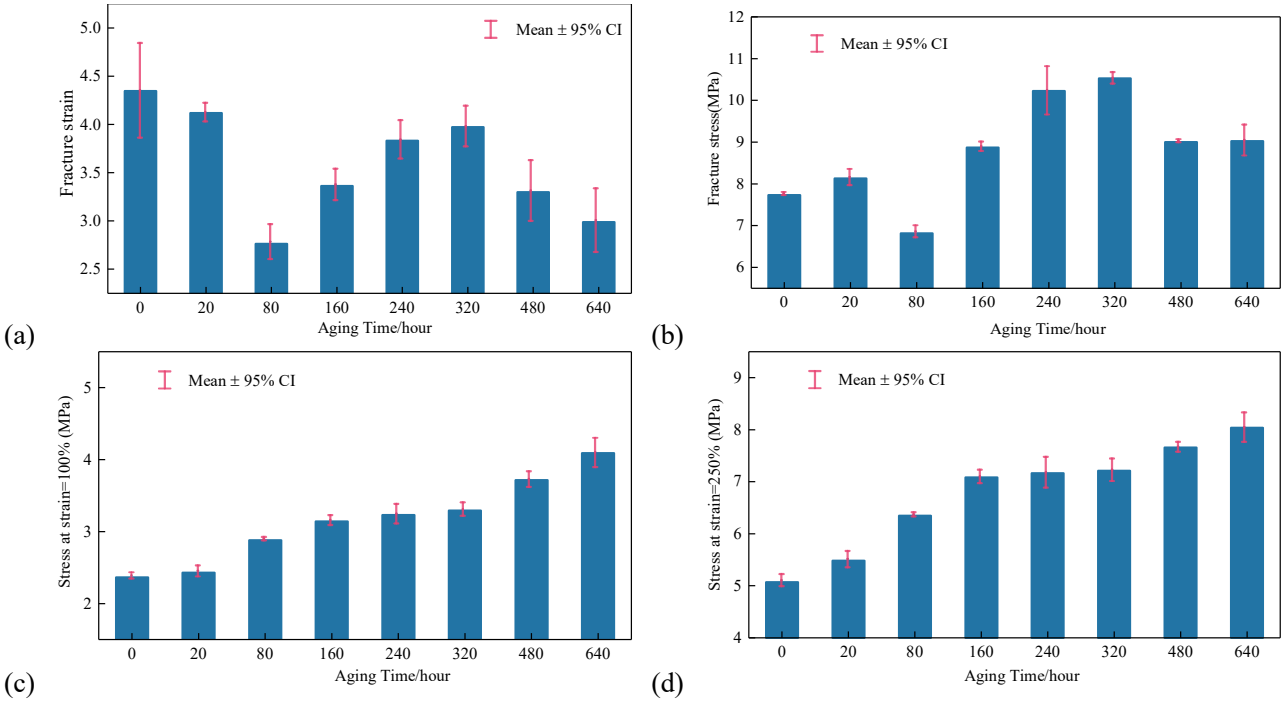

Figure 5 Statistical means of characteristic parameters for VEMs under different aging time: (a) Fracture strain; (b) Fracture stress; (c) Stress at strain=100%; (d) Stress at strain=250%.

Table 2 Statistical means of characteristic parameters of aging VEMs

Characteristic parameter	t_1 (h)	0	20	80	160	240	320	480	640
ε_f	Mean	4.34	4.12	2.76	3.36	3.83	3.97	3.30	2.99

	MSE	0.064	0.003	0.009	0.007	0.011	0.012	0.026	0.029
	Variance	0.097	0.004	0.013	0.011	0.016	0.018	0.040	0.044
	Mean	7.73	8.13	6.82	8.87	10.22	10.52	9.00	9.02
σ_f (MPa)	MSE	0.004	0.117	0.064	0.039	1.034	0.059	0.005	0.422
	Variance	0.006	0.176	0.096	0.059	1.552	0.089	0.007	0.633
	Mean	2.36	2.43	2.88	3.14	3.23	3.29	3.72	4.09
$\sigma_{100\%}$ (MPa)	MSE	0.006	0.018	0.002	0.015	0.057	0.027	0.037	0.128
	Variance	0.009	0.028	0.003	0.022	0.086	0.040	0.056	0.192
	Mean	5.07	5.48	6.35	7.08	7.16	7.21	7.66	8.04
$\sigma_{250\%}$ (MPa)	MSE	0.042	0.076	0.004	0.053	0.271	0.143	0.028	0.248
	Variance	0.063	0.115	0.007	0.080	0.406	0.215	0.042	0.372

During TO aging, the secondary oxidation cross-linking (SOC) reaction which generates new cross-link points and the chain scission (CS) reaction which destroy cross-link points, as illustrated in Figure 6, take place simultaneously albeit at different rates [14, 15, 28]. Due to the coupled effects of SOC reaction and CS reaction, the overall regularity of chain network changes and the stress-strain transmission capacity of the chain structure in general deteriorates [15, 39].

It is likely at early aging, SOC may happen more than CS due to the unsaturated free radicals in VEMs may react with oxygen and heat, resulting in a denser network. This has the effect of decreasing the fracture strain and increasing the stress at fracture [2, 18, 40]. Beyond a certain age (such as 80 h), CS may happen more often as it ages with the SOC continuing to be formed with some of the links in a direction highly oblique to the load path. This has the effect of lengthening the effective chain length with lesser chain along the load path, leading to an increase in fracture strain and decrease in fracture stress as shown in Figure 5(a) and (b). The SOC may continue to form as aging takes place at a rate faster than CS again forming a dense network, which may explain the decrease in fracture strain and increase in fracture stress. Beyond 320 h, network density may be saturated due to continuous consumption of unsaturated free radicals, with CS continuing to take place which explains the decrease

in fracture stress[40, 41]. There is the possibility that anomaly in the results may occur due to the presence of some internal defects in these two-groups of specimens, which may be amplified by TO aging, although this is unlikely given that the results are the average of 5 specimens.

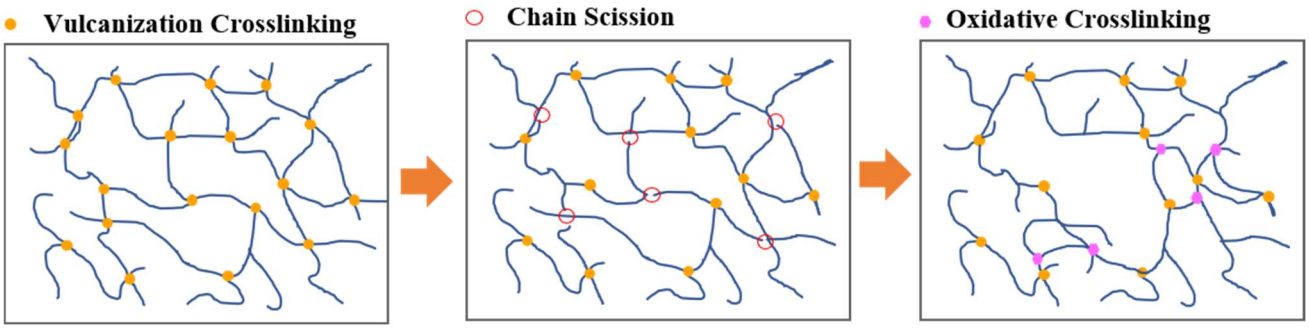

Figure 6 Alteration of molecular chain network of VEMs during thermal-oxidative aging

Figure 5 (c) and (d) show that $\sigma_{100\%}$ and $\sigma_{250\%}$ significantly increase with t_1, and their increase rates show a downward trend. For example, when t_1 increases from 0 h to 240 h, $\sigma_{100\%}$ increases from 2.36 MPa to 3.23 MPa and $\sigma_{200\%}$ increases from 5.07 MPa and 7.16 MPa, with an increment of 0.004 MPa and 0.009 MPa per hour, respectively. In comparison, when t_1 increases from 320 h to 640 h, $\sigma_{100\%}$ increases from 3.29 MPa to 4.09 MPa and $\sigma_{250\%}$ increases from 7.21 MPa and 8.04 MPa with an increment of 0.002 MPa and 0.003 MPa per hour, respectively. This phenomenon can be explained by the formation of new cross-linking structure between molecular chains during TO aging, which results in the increase of the binding bonds and the decrease of the effective length of a single molecular chain, and finally improves the entropic elasticity of a single molecular chain [18, 41]. However, with the continuous consumption of unsaturated free radicals, the rate of SOC reaction slows down, which finally leads to the decline of the increase rate of stress.

3 Mechanical property characterization of thermal-oxidative aging VEMs

3.1 Mechanical behavior description based on microsphere theory

The microsphere theory holds that the chain structure of rubber polymer is a 3-D topological network composed of infinite 1-D subnetworks with unique orientations in space [15, 42, 43]. The mechanical properties of chain network can be characterized by numerically integrating the strain energy of subnetworks on the whole sphere [44, 45], expressed is

$$\Psi = \frac{1}{M_s}\int \phi^q d^q u \cong \sum_{j=1}^{k} \omega_j \phi^{q_j} \tag{1}$$

where Ψ is the strain energy of rubber polymer, M_s is the surface area of microsphere S, $d^q u$ is the infinitesimal area in direction q, ω_j is the weight in direction q_j, ϕ^{q_j} is the strain energy of molecular chains in direction q_j, k is the number of integration points.

To describe the strain energy of a single molecular chain ϕ, [46] proposed a modified Kuhn-Grün model given by

$$\phi(n,\bar{r}) = nk_0T_0\int_0^{\tau}\hat{\beta}\,(\tau,n)d\tau + \phi_0, \qquad \hat{\beta}(\tau,n) = \left[1-\frac{1+\tau^2}{n}\right]\beta \tag{2}$$

where n is the number of Kuhn segments on a single chain, k_0 is the Boltzmann constant, T_0 is the absolute temperature, ϕ_0 is a constant, $\tau = r/nl$ is the extensibility ratio in the deformed configuration where r and l are the end-to-end distance and length of a single Kuhn segment, $\beta = \mathcal{L}^{-1}(\tau)$ is the inverse Langevin function of elongation ratio, and can be approximated as [47]

$$\beta = \mathcal{L}^{-1}(x) \cong \frac{1}{1-x} + x - \frac{8}{9}x^2 \tag{3}$$

in which x is the independent variable.

For VEMs, the molecular chain structure is complex with different types of chains such as elastic chains and free chains [30]. Elastic chain refers to the molecular chain forming a complete cross-linking network, and can transfer stress and strain to each other. The free chain mainly includes the molecular chain without cross-linking network, which cannot transfer stress and strain. When describing the mechanical behavior of VEMs, the total strain energy of chain structure can be decoupled into the superposition of contributions from the elastic chain layer and the free chain layer, as shown in Figure 7.

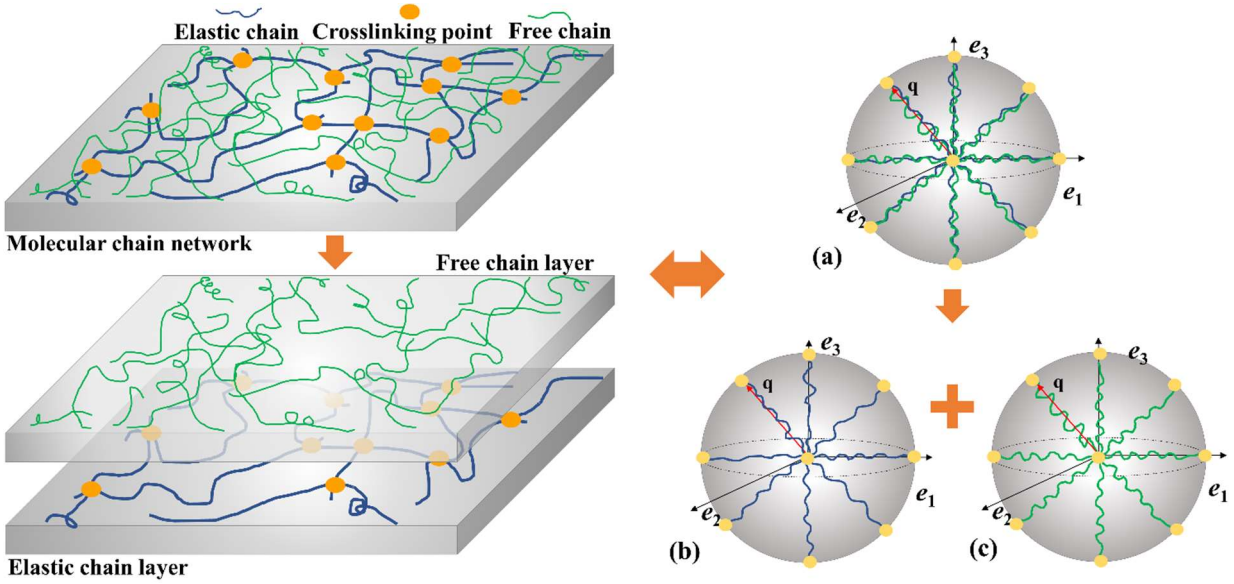

Figure 7 Decoupling of microstructure of VEMs: microsphere models for characterizing (a) whole network chain, (b) elastic chain, and (c) free chain.

Based on equations (1)~(2), the strain energy of the elastic chains and free chains for unaged VEMs, denoted as $\widehat{\Phi_e}$ and $\widehat{\Phi_f}$, can be expressed as

$$\widehat{\Phi_e} = \sum_{j=1}^{k} N_e \omega_j \, \phi^{q_j}(n, \bar{r}) \tag{4}$$

$$\widehat{\Phi_f} = \sum_{j=1}^{k} N_v \omega_j \, \phi^{q_j}(n, \bar{r}) \tag{5}$$

where N_e and N_v are the molecular chain density of elastic chain and free chain in unit volume. Note that in this paper, variables with the superscript $\widehat{\ }$ represent the corresponding physical quantities of the unaged VEMs, $\bar{r}$ is the end-to-end distance normalized by l.

The total strain energy of unaged VEMs $\widehat{\Phi}$ is then expressed as

$$\widehat{\Phi} = \widehat{\Phi_e} + \widehat{\Phi_f} \tag{6}$$

3.2 Effect of thermal-oxidative aging on chain network of VEMs

Under TO condition, the SOC reaction and CS reaction may affect the mechanical behavior of VEMs in a superposed manner [14, 15]. In this section the changes of elastic chain and free chain under TO aging will be analyzed and theoretically characterized.

(1) ***Effect of TO aging on elastic chain***

Under the action of SOC reaction and CS reaction, the elastic chain may form or lose crosslinking points, mainly under the following cases:

i) SOC reaction occurs between two elastic chains with one new crosslinking point forming, as shown in Figure 8(a). The number of elastic chains increases from 2 to 4, and the effective length of original elastic chains becomes shorter;

ii) SOC reaction occurs between the elastic chain and free chain with new crosslinking point forming, as shown in Figure 8(b). As one new crosslinking point formed, the changes of number and length of an elastic chain is like those in i), the number of free chains involved increases from 1 to 2 with shorter effective length;

iii) SOC reaction occurs between the elastic chain and free chain with more than one new crosslinking points forming, as shown in Figure 8(c). As two new crosslinking points formed, the original elastic chain is divided into three new elastic chains with shorter length, partial free chain between such two crosslink points is converted into elastic chain whereas the rest becomes two free chains with shorter length;

iv) CS reaction occurs in the elastic chain network, as shown in Figure 8(d). During this process, the original crosslinking points in the chain network are destroyed, thus converting the related elastic chains into free chains.

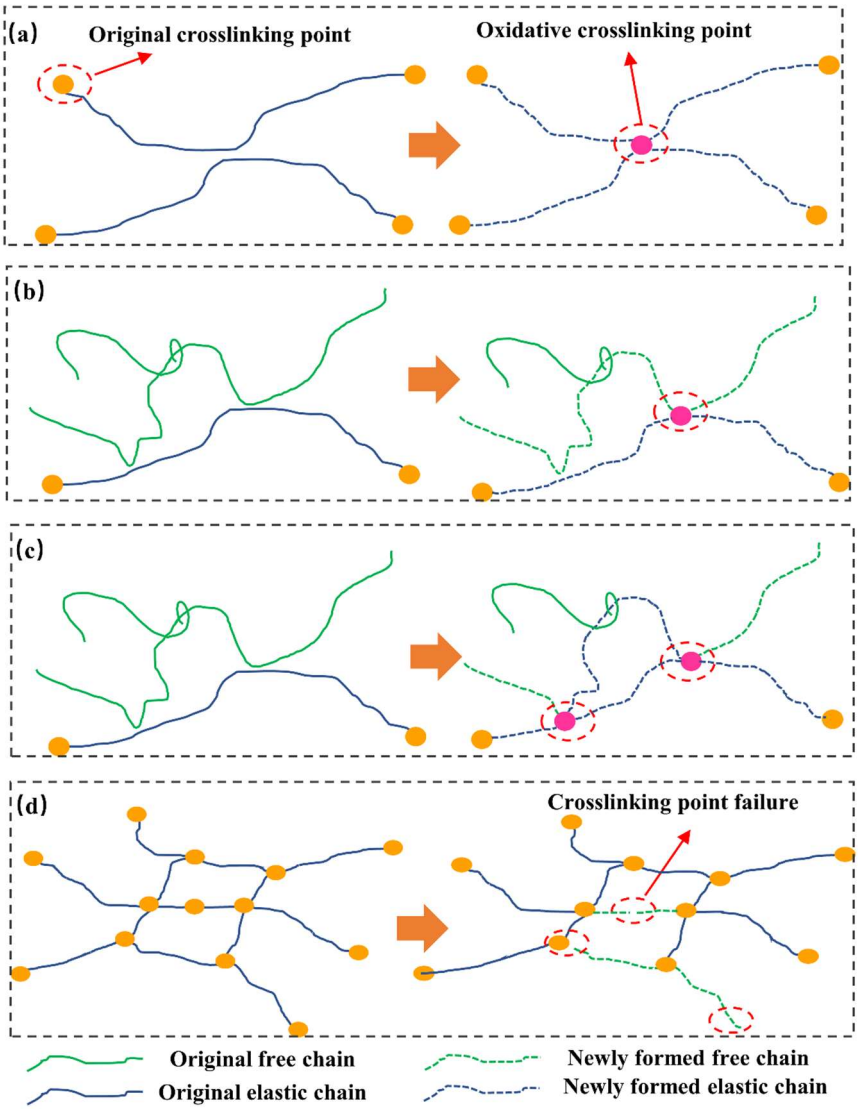

Figure 8 Alterations of elastic chain by chemical reactions during thermal-oxidative aging; (a)~(c) SOC reaction; (d) CS reaction.

From the above analysis, the elastic chains during aging can be divided into two types: i) the original elastic chains without aging; ii) the newly formed elastic chain during aging.

If the proportion of the unaged molecular chains to the total molecular chains at t_1 is κ, the total strain energy of the elastic chains Φ_e can be obtained as

$$\Phi_e = \Phi_{e0} + \Phi_{e1} \tag{7}$$

where Φ_{e0} is the strain energy of unaged elastic chains, which can be determined as

$$\Phi_{e0} = \kappa \sum_{j=1}^{k} N_e \omega_j \phi^{q_j}(n, \bar{r}) \tag{8}$$

Since the relationship of chemical reaction with reaction time and reaction temperature, κ should be the function of t_1 and T. Considering the changes of CS reaction and SOC reaction on the macroscopic mechanical behavior of VEMs, the aging function κ may be constructed as [15]

$$\kappa = (A_f \rho_f + A_s \rho_s) \tag{9}$$

where A_f and A_s can be regarded as the weight coefficient of SOC reaction and CS reaction, satisfying $A_s + A_f = 1$, $\rho_{(\blacksquare)}$ is the corresponding influence function, and subscript $(\blacksquare)$ represents either s and f corresponding to CS reaction and SOC reaction respectively. Assuming that reactions in the TO aging are all first-order reactions [15], $\rho_{(\blacksquare)}$ theoretically can be characterized as

$$\rho_{(\blacksquare)} = exp\left(-\delta_{(\blacksquare)} e^{-\frac{E_{a,(\blacksquare)}}{RT_{ref}}} a_{T,(\blacksquare)} t_1^{ref}\right) \tag{10}$$

where $\delta_{(\blacksquare)}$ is the pre-exponential factor, $E_{a,(\blacksquare)}$ is the activation energy, $R = 8.314 JK^{-1}mol^{-1}$ is the ideal gas constant, T and T_{ref} are the actual reaction temperature and reference temperature,

respectively, t_1^{ref} is the reference aging time, $a_{T,(\blacksquare)}$ is the aging time-temperature shift factor, given by

$$a_{T,(\blacksquare)} = exp\left(\frac{E_{a,(\blacksquare)}}{R}\left(\frac{1}{T_{ref}} - \frac{1}{T}\right)\right) \tag{11}$$

As can be seen from Figure 8(a)~(c), the number of new crosslinking points on the original elastic chain is consistent with the number of newly generated elastic chains. If the probability of forming a new crosslinking point on a single chain during aging is P_f, the probability of forming *m* cross-linking points on a single elastic chain is $P_{\mathrm{f}}^{\mathrm{m}}$.

From the perspective of statistical distribution of the overall elastic chain, since the number of elastic molecular chains is very large, it can be deduced that the TO aging does not change the statistical distribution of newly formed elastic chains. If the average number of crosslinking points generated on an aging elastic chain is m_e, and m_e newly generated crosslinking points equally divide the original elastic network chain, the strain energy of the elastic chains formed from the original elastic chains due to the SOC reaction, denoted as Φ_{e11}, is given by

$$\Phi_{e11} = (1-\kappa)\sum_{j=1}^{k} N_e P_f^{m_e} \omega_j \, (m_e + 1)\phi^{q_j}(n, \bar{r}) \tag{12}$$

On the other hand, during the TO aging, free chains can also be transformed into elastic chains, as shown in Figure 8(b)~(c) and Figure 9. If the average number of crosslinking points generated on an aging free chain is m_f, based on equation (12), the strain energy of the elastic chains transformed from the free chains, denoted Φ_{e12}, can be expressed as

$$\Phi_{e1} \ = (1-\kappa)\sum_{j=1}^{k} N_v P_f^{m_f} \omega_j \left(m_f - 1\right)\phi^{q_j}(n, \bar{r}) \tag{13}$$

The strain energy of elastic chain layer Φ_e is thus modified as

$$\Phi_e = \Phi_{e0} + \Phi_{e11} + \Phi_{e12} \tag{14}$$

(2) ***Effect of TO aging on free chain***

In the TO aging, the free chains may also undergo SOC reaction with surrounding free chains to generate new cross-linking points. Along a free chain, when more than one new crosslinking points are formed, each segment between the neighboring new points will be converted into an elastic chain, as shown in Figure 9. In the case of CS reaction which mainly refers to the destruction of the cross-linking points between the elastic chains, its influence of CS reaction on the free chain is ignored here.

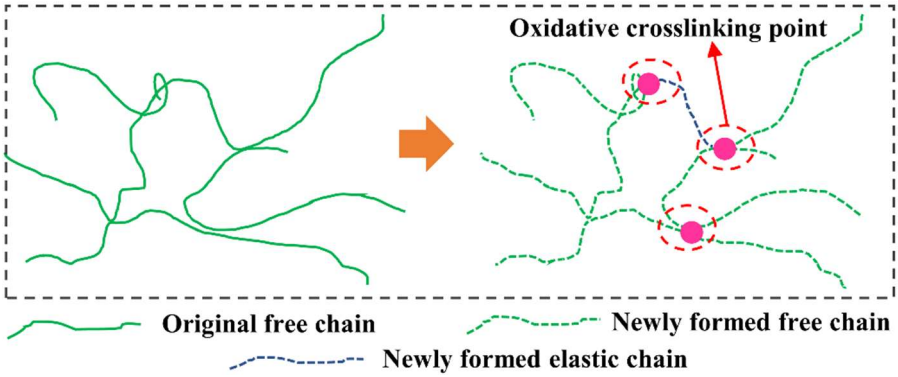

Figure 9 Alteration of free chain by SOC reaction during thermal-oxidative aging

As with elastic chains, the free chains during aging can be divided into two types: i) the original free chains without aging; ii) the newly formed free chain during aging.

Strain energy of the whole free chains Φ_f is represented as

$$\Phi_f = \Phi_{f0} + \Phi_{f1} \tag{15}$$

where the strain energy of unaged free chains Φ_{f0} is expressed according to equation (5), as

$$\Phi_{f0} = \kappa \sum_{j=1}^{k} N_v \omega_j \phi^{q_j}(n, \bar{r}) \tag{16}$$

As observed from Figure 8(d), CS reaction can destroy the original crosslinking points on the elastic chain network, and transfer elastic chains into free chains. If there are h elastic chains with the same configuration connected to a crosslinking point on average, and the probability of losing a crosslinking point on a single elastic chain is P_s, the strain energy of free chains generated from elastic chains during aging, denoted Φ_{f1}, can be expressed as

$$\Phi_{f11} = (1-\kappa)\sum_{j=1}^{k} N_e P_s \omega_j \, h\phi^{q_j}(n,\bar{r}) \tag{17}$$

On the other hand, one can conclude form Figure 8(a)~(c) and Figure 9 that when m_f new crosslinking points are generated on a free chain averagely, the parts at both ends of free chain will be converted into two new free chains, although other parts are converted into elastic chains. The strain energy of free chains formed from the original ones, Φ_{f12}, is given by

$$\Phi_{f12} = (1-\kappa)\sum_{j=1}^{k} 2N_v P_f^{m_f} \omega_j \, \phi^{q_j}(n,\bar{r}) \tag{18}$$

The strain energy of free chain layer Φ_f is thus modified as

$$\Phi_f = \Phi_{f0} + \Phi_{f11} + \Phi_{f12} \tag{19}$$

The strain energy of TO aging VEMs denoted Φ can be determined as

$$\Phi = \Phi_e + \Phi_f \tag{20}$$

3.3 Mathematical model of thermal-oxidative aging VEMs

Different additives are often added into the rubber matrix to improve its mechanical performance, making the molecular chain structure of VEMs complex. To further understand the microstructure of

VEMs, the actual micromorphological structures of the test samples with different t_1 are scanned by electron microscope (Sigma 300, Zeiss Corporation, Germany) as shown in Figure 10 (a) and (c).

To comprehend the distribution state between the matrix rubber and additives, the pixel processes are conducted on the entire region of SEM images, and the results are shown in Figure 10 (b) and (d), where the black portions indicate the additives, and the white portions is the rubber matrix. Furthermore, to examine the impact of TO aging on the volume content of additives in VEMs, the grayscale analyses are performed on the whole region of pixel processing results (namely, on the entire regions within the box of Figure 10 (b) and (d)), the area proportion of rubber matrix and additives are calculated to quantitatively describe the volume content of additives before and after aging, as listed in Table 3.

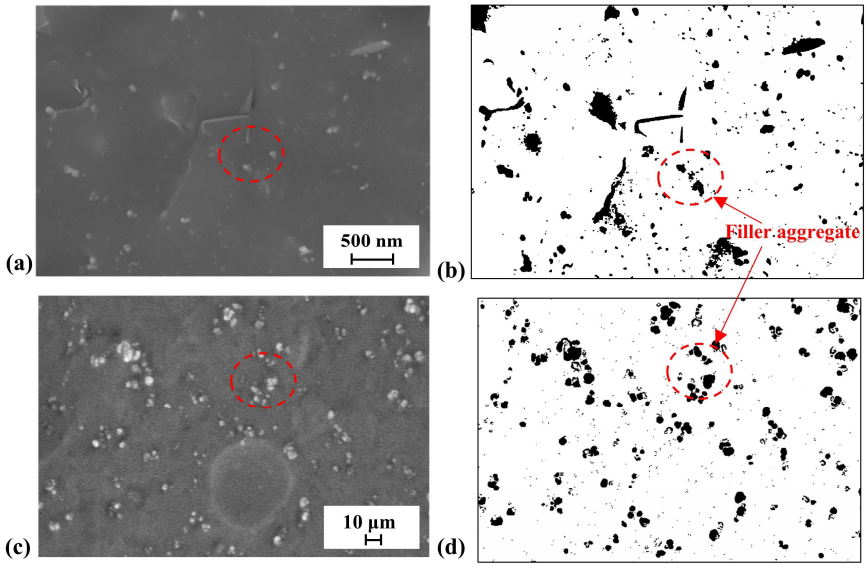

Figure 10 Actual micromorphology and corresponding pixel processing results of VEMs fracture section for: (a)~(b) $t_1 = 0h$; and (c)~(d) $t_1 = 640h$

Table 3 Area proportion of rubber matrix and additives before and after aging

Aging time (h)	Area ratio (%)		Change rate of additives (%)
	Rubber matrix	Additives	
0	93.43	6.57	4.57

640	93.13	6.86	

The random and discrete distribution of different additives in the matrix with obvious aggregation in Figure 10 may lead to significant non-uniformity of the material stiffness. Between aging time of 0 h and 640 h, the uneven state of the additive distribution has not been changed significantly. Quantitatively, as seen from Table 3, remarkable variation of content of additives during aging process has not been observed as the volume contents of additives before and after aging are no more than 5%. This may be because the additives primarily comprise compounds with stable chemical properties, such as zinc oxide, carbonates, and silicates, etc., which are less easily to react with oxygen or other media under TO conditions compared to those more active unsaturated groups in molecular chain network of VEMs such as hydrogen bonds and other free radicals [18, 37].

To consider this heterogeneity, a strain amplification function is employed, and a non-affine directional model by considering the non-uniformity of deformation distribution is proposed [29], which is

$$\lambda^{q_j} = \frac{\chi^{q_j} - \mu^{\nu}}{1 - \mu^{\nu}} \tag{21}$$

Where $\lambda^{q_j} = (q_i \mathbf{F}^{\boldsymbol{T}} \mathbf{F} q_i)^{1/2}$ and χ^{q_j} are the microscopic tensile ratio and the macroscopic tensile ratio in direction q_j, in which $\mathbf{F}$ is the deformation gradient, μ is the volume fraction of filler in the range of 0~0.3, ν depends on the matrix network, and is taken as 1/3 in this paper [48].

To consider the reinforcing effect of filler on the rubber matrix, the filler-reinforcement coefficient γ is introduced here to modify the stress of unfilled system, given by [32]

$$\gamma = \begin{cases} 1 + 2.5\mu + 14.1\mu^2 & \mu < 0.3 \\ [1/(1 - \mu/\mu_{max})]^{2.5\mu_{max}} & \mu > 0.3 \end{cases} \tag{22}$$

Based on equation (20), the first Piola-Kirchhoff stress tensor $\mathbf{S}$ of the aging VEMs is obtained as:

$$\boldsymbol{S} = \gamma\left(\frac{\partial \Phi(\boldsymbol{F})}{\partial \boldsymbol{F}} - p\boldsymbol{I}\boldsymbol{F}^{-\mathbf{1}}\right) \tag{23}$$

where p is an arbitrary scalar to satisfy the boundary condition, $\mathbf{I}$ is the unit matrix and

$$\frac{\partial \Phi_{(\blacksquare)}(\boldsymbol{F})}{\partial \boldsymbol{F}} = \sum\nolimits_{j=1}^{k} \omega_j \frac{\partial \phi_{(\blacksquare)}^{q_j}}{\partial \lambda^{q_j}} \frac{\partial \lambda^{q_j}}{\partial \chi^{q_j}} \frac{1}{2\chi^{q_j}} \frac{\partial \chi^{q_j}}{\partial \boldsymbol{F}} \tag{24}$$

$$\left.\frac{\partial \phi(n,x)}{\partial x}\right|_{x=\lambda^{q_j}} = \sqrt{n} k_0 T_0 \hat{\beta}\left(\frac{\lambda^{q_j}}{\sqrt{n}}, n\right) \tag{25}$$

$$\frac{\partial \chi^{q_j}}{\partial \boldsymbol{F}} = \frac{\partial q_j \overline{\boldsymbol{C}} q_j}{\partial \boldsymbol{F}} : \frac{\partial \overline{\boldsymbol{F}}}{\partial \boldsymbol{F}} = 2\boldsymbol{J}^{-\frac{\mathbf{1}}{\mathbf{3}}} \overline{\boldsymbol{F}}(q_i \otimes q_i) \tag{26}$$

in which $\overline{\boldsymbol{F}}$ is $\boldsymbol{F}$ normalized by l, $\mathbf{C}$ is the right Cauchy green tensor, $\mathbf{J^2 = detC}$ and $\bar{\mathbf{C}} = \mathbf{J^{-2/3}C}$.

4 Evaluation on predictive capability and adaptability of proposed Model

To widen the evaluation on the prediction accuracy and robustness of proposed model under different testing conditions, besides our own test data, another two sets of data were extracted from [14, 28] and used for verification. The 3 sets of data formed cases 1 (test data in Section 2), cases 2 (test data in literature [28]), and cases 3 (test data in literature [14]). The prediction using the aging microsphere model is compared with those using the proposed model. A note on the derivation of the aging microsphere model is explained in Appendix A.

The microsphere model is evaluated numerically using 21 integration points on the hemisphere considering the computational accuracy and efficiency, which has been proved to be capable of reflecting the mechanical behavior of VEMs [14, 49, 50].

The physical-chemical parameters of the proposed model are calibrated prior to the verification, which is described in [34]. Their values for the 3 cases of both models and their corresponding average fitting errors (AFEs) are listed in Table 4 and Table 5.

Table 4 Identified parameters and corresponding AFEs of proposed models

Data group		Case 1	Case 2	Case 3
Model parameter	A_s	0.925	0.106	0.100
	P_f	0.029	0.835	0.102
	P_s	0.405	0.100	0.100
	N_e	2.00×10^{22}	6.20×10^{20}	1.00×10^{21}
	N_v	5.28×10^{22}	3.60×10^{22}	1.00×10^{21}
	n	67.750	408.475	1.49×10^{5}
	$E_{a,s}/R$	802.927	5.32×10^{3}	4.77×10^{3}
	$E_{a,f}/R$	1.127	5.94×10^{3}	6.54×10^{3}
	m_e	64.387	4.567	1.64×10^{4}
	m_f	42.692	1.842	1.01
	h	14.058	927.1	0.103
	δ_s	0.057	1.18×10^{4}	-9.52×10^{4}
	δ_f	3.896	1.88×10^{5}	-4.73×10^{6}
	T_{ref}	-18.405	3.32×10^{10}	-7.38×10^{6}
AFE (%)		3.1	3.6	4.2

Table 5 Identified parameters and corresponding AFEs of aging microsphere models

Data group		Case 1	Case 2	Case 3
Model parameter	A_s	0.613	0.154	0.100
	N	9.21×10^{21}	1.14×10^{22}	1.20×10^{22}
	n	56.667	39.437	4.64×10^{3}
	$E_{a,s}/R$	2.67×10^{3}	74.586	1.63×10^{4}
	$E_{a,f}/R$	3.34×10^{3}	175.460	3.27×10^{4}
	δ_s	-0.871	64.007	-1.74×10^{19}
	δ_f	-5.425	-0.017	0.110
	T_{ref}	-9.152	319.152	2.99×10^{19}
AFE (%)		8.3	21.5	9.4

The AFEs of the proposed model for the 3 cases range from 3.1%~4.2% whereas the AFEs of the aging microsphere model range from 8.3%-21.5%, and are all over 8% with the maximum value of 21.5%. Thus, the proposed model provides a better description of the mechanical behavior of TO aging VEMs,

indicating that the modifications made on the original microsphere model gives significant improvements.

Based on the determined parameters, the results for the test data are predicted and depicted in Figure 11~Figure 13. The results for the 3 cases calculated by the proposed model agree well with those from experiments, whereas the aging microsphere model exhibits significant errors in predictions. For instance, the maximum prediction errors of the proposed model are 17.2%, 16.3%, and 15.6%, and those from the aging microsphere model are 17.8%, 31.2%, and 41.0%. Correspondingly, the average predicted errors (APEs) of the proposed model are 3.0%, 4.7%, and 8.5%, while those from the aging microsphere model are basically above 5% with the average of 9.3%.

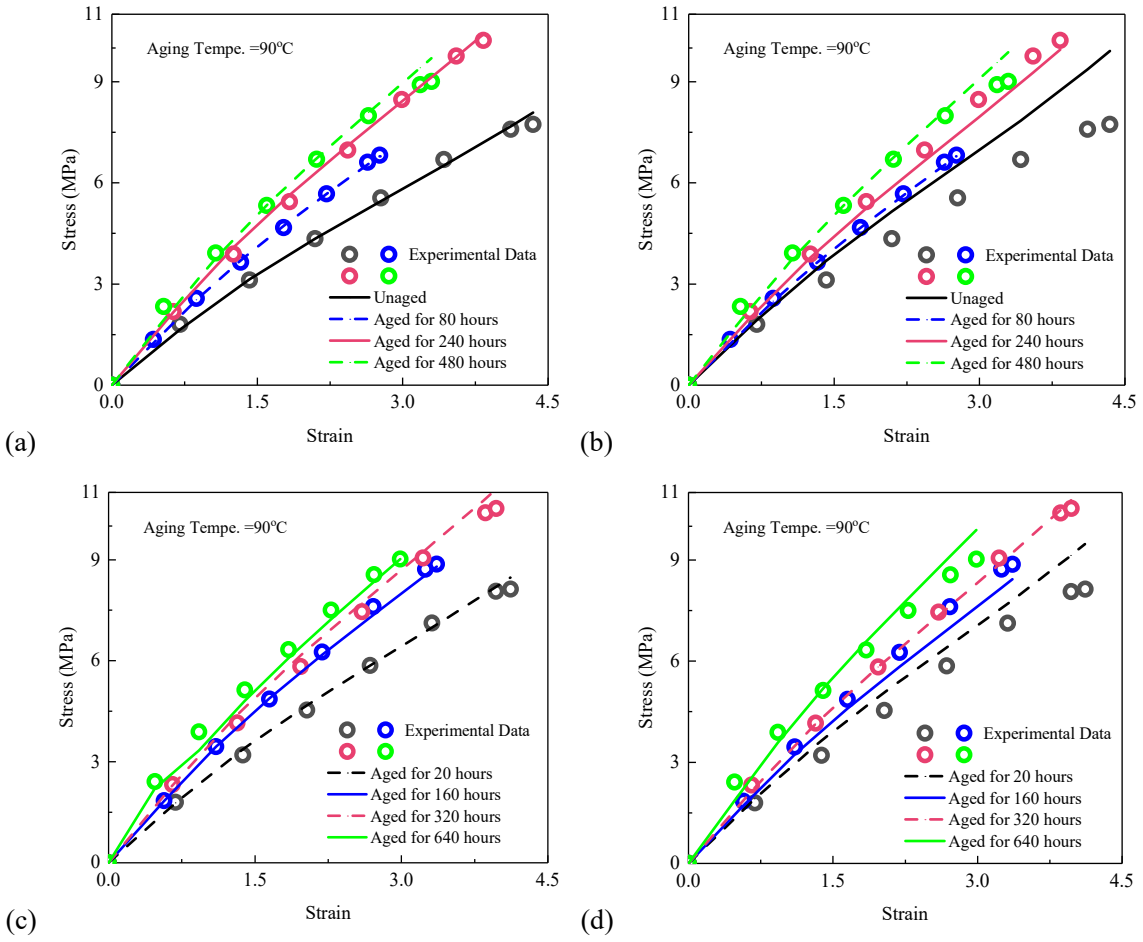

Figure 11 Results for aging VEMs of Case 1: (a), (c) proposed model; and (b), (d) aging microsphere model. Discrete symbols depict experimental data. Solid lines exhibit fitted results, and dotted lines show predicted result from mathematical models.

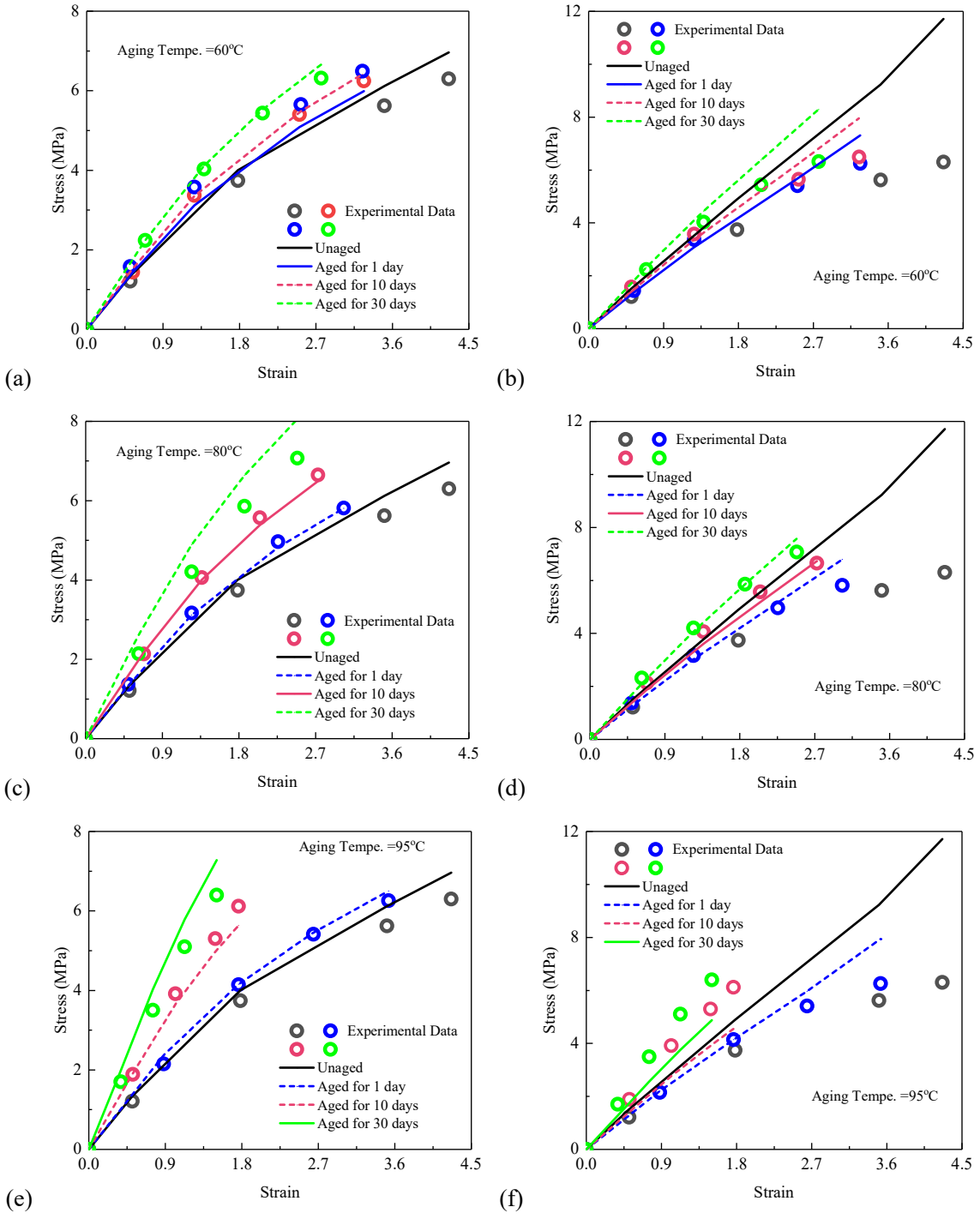

Figure 12 Results for aging VEMs of Case 2: (a), (c) and (e) proposed model; and (b), (d) and (f) aging microsphere model. Discrete symbols depict experimental data. Solid lines exhibit fitted results, and dotted lines show predicted result from mathematical models.

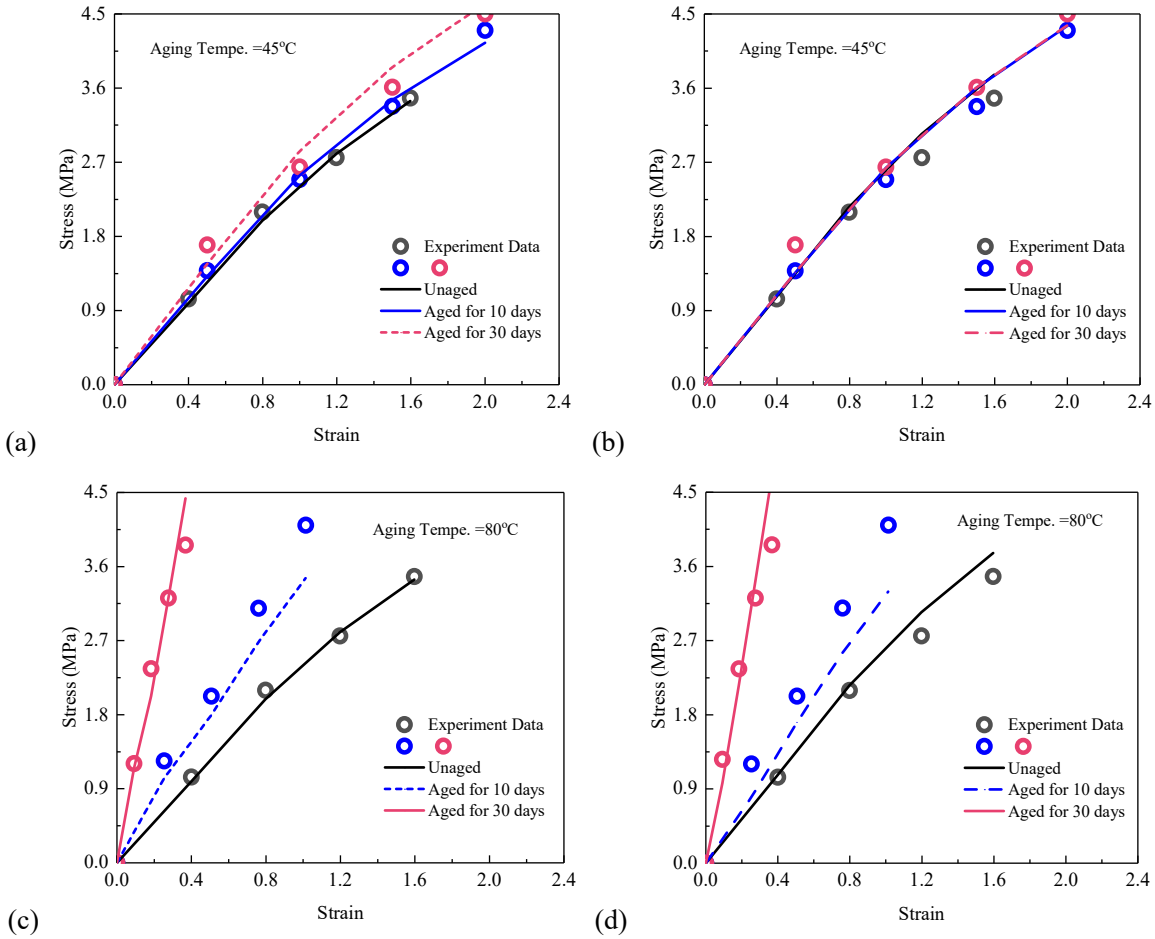

Figure 13 Results for aging VEMs of Case 3: (a), (c) proposed model; and (b), (d) aging microsphere model. Discrete symbols depict experimental data. Solid lines exhibit fitted results, and dotted lines show predicted result from mathematical models.

Error analyses are also carried out for the predicted results using the determination coefficient R^2 and the residual ϵ, as listed in Table 6. As observed, R^2 of the prediction results by the proposed model range from 0.965 to 0.995 whereas those from the aging microsphere model are 0. 895 to 0.963. The absolute values of average residuals for the proposed model are less than 0.12, whereas those of the aging microsphere model range from 0.14 to 0.31.

Table 6 Error analyses on predicted results of the proposed model (PM) and comparative model (CM)

Data group	Maximum PE (%)		APE (%)		R^2		ϵ	
	PM	CM	PM	CM	PM	CM	PM	CM
Case 1	**17.2**	17.8	**3.0**	4.7	**0.994**	0.982	**-0.103**	-0.166
Case 2	**16.3**	31.2	**4.7**	10.1	**0.977**	0.895	**-0.035**	-0.137

Case 3	**15.6**	41.1	**8.5**	13.1	**0.965**	0.918	**0.111**	0.310

* Bold is the relatively best

In addition, one can see from Figure 13(b) that the predicted results given by the aging microsphere model shows significant aggregation. This is because the stress-strain changes of VEMs are indistinctive under different aging time at this working condition. In general, compared with the aging microsphere model, the proposed model exhibits a better prediction capacity and robustness under different TO aging conditions. This is because the aging microsphere model can only make rough statistics of the molecular chains and fails in distinguishing the alteration of different-kind chains of aging VEMs caused by different aging reactions. Also, the filler-reinforcement effect and non-affine assumption involved in the proposed model contribute to the improvement of prediction capability.

5 Sensitivity analysis of model parameters

To better understand the influence of TO aging on the mechanical behavior of VEMs, a parameter sensitivity analysis is conducted on the proposed model. For the proposed model, considering that some parameters have no physical significance or have been extensively studied [15], the model parameters chosen in the present sensitivity analysis include: i) mechanical parameters N_{e}, N_v, n; ii) aging parameters A_{s}, P_f, P_s, m_e, m_f, h.

The model parameters of Case 1 given in Table 4 are taken as the reference values, and the reference test condition with T = 90 ºC and t_1 = 320 h is selected. In the calculation process, the reference values of the specific parameters to be studied is employed as the benchmark for adjustment. The calculated results are plotted in Figure 14 and Figure 15, in which η_e denotes the contribution ratio of elastic chain to total stress of TO aging VEMs.

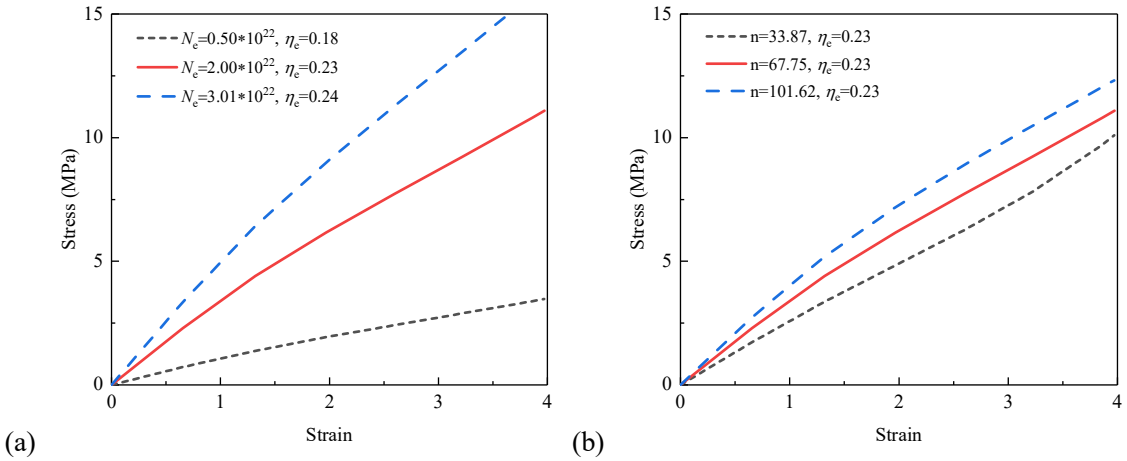

Figure 14 Sensitivity analyses on mechanical parameters of proposed model.

With the increase of N_e, the stress level and tangent modulus of VEMs demonstrate a significant increasing trend with the increase in η_e. This is because the macroscopic elasticity of VEMs is positively correlated with elastic chains, and the increase in elastic chains can directly result in their increasing contribution to the total stress of VEMs. The stress level of VEMs increases with the increase in n. This can be explained by the fact that higher n means higher degree of curl and entropic elasticity, which results in higher stress levels. In addition, since the enhancement of entropic elasticity acts on both elastic chain and free chain, the contribution ratios of these two kinds of chains to the total stress remain unchanged.

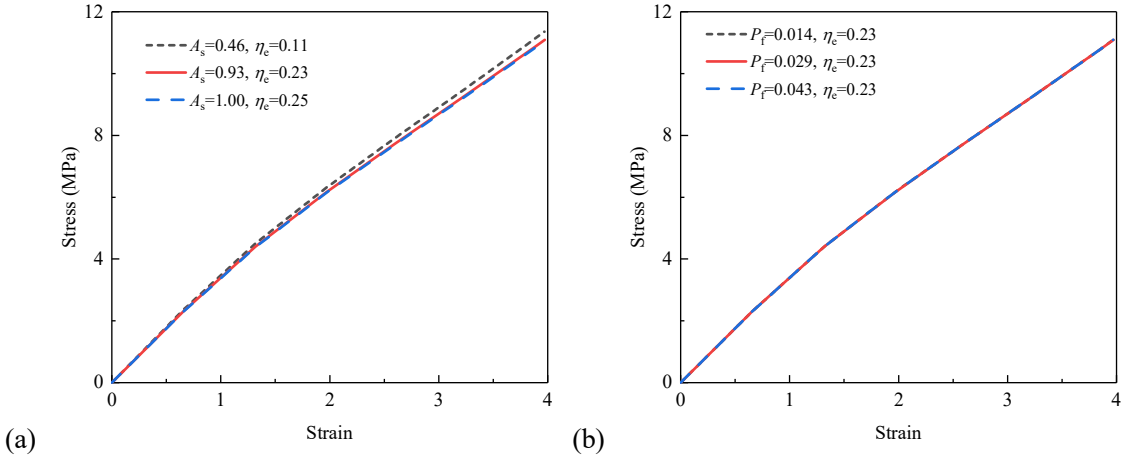

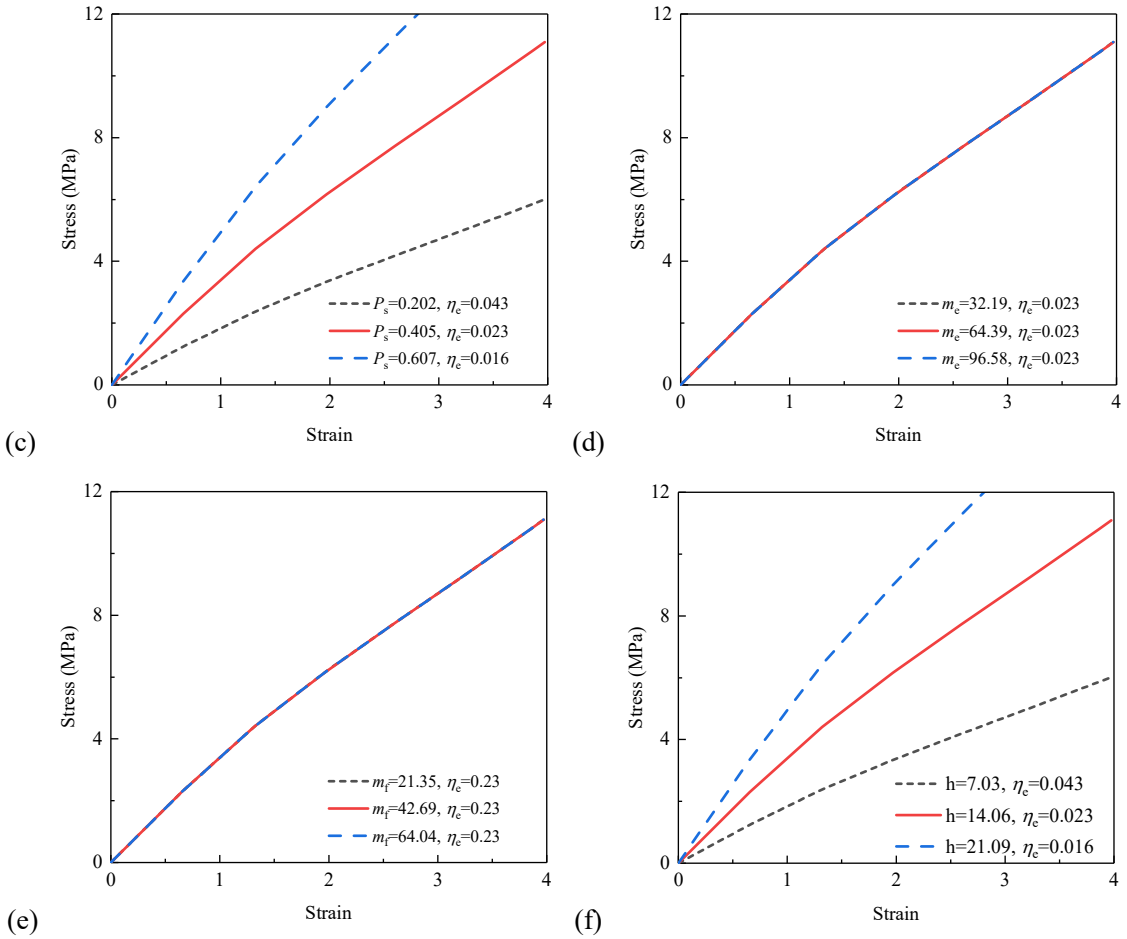

Figure 15 Sensitivity analyses on aging parameters of proposed model.

As seen from Figure 15 (a), with the increase in A_s, the stress level of the material shows a decreasing trend with an obvious increment in η_e observed. This is because the destruction to the crosslink points of elastic chain increases with the growth of proportion of SC reaction in total reaction, leading to the damage to the whole chain network and the following modulus degradation of the material. On the other hand, since that the decrease in total stress of VEMs caused by losing elastic chains do not exceed the increase in total stress of VEMs caused by the newly formed free chains, η_e presents an increasing trendy.

Besides, one can observe from Figure 15 (b), (d), and (e) that the stress level of VEMs does not vary with the increase in P_f, m_e and m_f. This may be because that the probability of forming a new

crosslinking point on a single chain is less than 1, whereas the average number of forming a new crosslinking point on a single elastic chain or free chain is relatively large (much more than 1) since that the SOC reaction are often predominant during the TO aging [15, 18, 29, 51], which leads to the corresponding strain energy components including Φ_{e11}, Φ_{e12}, and Φ_{f12} are insensitive to the variations of P_f, m_e and m_f, which finally explain phenomenon presented in Figure 15 (b), (d), and (e).

Figure 15 (c) shows that VEMs exhibits an increase in stress level when increasing P_s, whereas η_e has a negative correlation with P_s. The is because that with the increase of the probability of losing a crosslinking point, more and more elastic chains will be converted into free chains, so that the contribution of elastic chains to total stress decreases. When the contribution of the newly formed free chains to the total stress of VEMs always exceeding the contribution from the vanished elastic chains, VEMs will show the phenomenon of stress increase. Figure 15 (f) shows that the stresses in VEMs are greatly improved by h, whereas η_e shows a decrease trend with increasing h. The reason is that more elastic chains linked to a single cross-linking point suggests more elastic chains per unit volume and higher entropic elasticity of the whole chain network, resulting in a higher stress level of VEMs. However, more elastic chains connected to a crosslinking point means that more elastic chains can be transformed into free chains by destroying cross-linking points, leading to a decrease in the stress contribution of elastic chains.

6 Conclusions

In this paper, the effects of thermal-oxidative (TO) aging on the stress-strain behavior of viscoelastic materials (VEMs) are studied through a series of experiments, a mathematical model for describing mechanical behavior of TO aging VEMs is established and verified, a sensitivity analysis on parameters of the proposed model is carried out. The following conclusions are drawn:

(1) Under the coupling effect of CS reaction and SOC reaction, the overall regularity of chain network gets destroyed, the stress-strain transmission capacity between molecular chains becomes weakened, leading to the deformation capacity of VEMs in general deteriorate. During TO aging process, the SOC reaction seems like happening more than the CS reaction on the whole, making the chain network of VEMs become denser, resulting in the phenomenon of modulus hardening. The SEM results suggest that the distribution and volume content of additives in viscoelastic materials have not significantly changed before and after aging.

(2) A microscopic chain-based mathematical model that can consider the evolution of molecular chains of VEMs during TO aging was proposed and verified against three groups of experimental data, and the verification demonstrates that the proposed model provides a significantly improved prediction on the stress-strain behavior of VEMs at different aging conditions as compared to the aging microsphere model.

(3) From the parameter sensitivity analysis of the proposed model, the stress level of VEMs demonstrates a notably positive relationship with the mechanical parameters N_{e}, n, and aging parameters P_s, h, and is negatively affected by the aging parameters A_{s}, whereas the stress-strain behaviors of VEMs are insensitive to changes in aging parameters P_f, m_e, and m_f.

(4) It should be noted that the actual molecular chain structure of VEMs is very complicated after TO aging. The proposed model has been established to include the main influencing factors, in which several simplifications have been involved. Nevertheless, as obtained from the verification results in Section 4, the proposed model can predict the stress-strain behavior of VEMs (more specifically, the Nitrile Butadiene Rubber-based VEMs) after TO aging with significant accuracy. In future study, the importance of the above-mentioned simplifications can be further examined and the corresponding effects may be incorporated in the model to further enhance its predictive capacity.

Appendix A. The aging microsphere model

According to equations (4) and (5), without distinguishing different-type molecular chains, the strain energy of unaged VEMs denoted $\widehat{\Phi}$ can be expressed based on the original microsphere model, as

$$\widehat{\Phi} = \int \phi(n,\bar{r})\, dn \cong \sum_{j=1}^{k} N\omega_j\, \phi^{q_j}(n,\bar{r}) \tag{A.1}$$

Furthermore, considering the effect of thermal-oxidative aging through equations (10)~(9), the strain energy of aging VEMs denoted Φ is determined by

$$\Phi = \kappa \int \phi(n,\bar{r})\, dn \cong \kappa \sum_{j=1}^{k} N\omega_j\, \phi^{q_j}(n,\bar{r}) \tag{A.2}$$

As the strain energy is given in (A.2), the aging microsphere model can be completed according to the derivation process described in Section 3.3.

Appendix B. Nomenclature

The following symbols are used in this paper:

ε_f, σ_f = The fracture strain and fracture stress;

$\sigma_{100\%}$, $\sigma_{250\%}$ = The stress at 100% strain and at 250% strain;

Ψ = The strain energy of rubber polymer;

M_s = The area of microsphere S;

$d^q u$ = The infinitesimal area in direction q;

ω_j, k = The weight in direction q_j and the number of integration points;

ϕ^{q_j} = The strain energy of molecular chains in direction q_j;

k_0, T_0 = The Boltzmann constant and the absolute temperature;

n = The number of Kuhn segments on a single chain;

β = The inverse Langevin function of elongation ratio;

r, $\bar{r}$ = The end-to-end distance before and after normalization;

l = The length of a single Kuhn segment;

τ = The extensibility ratio in the deformed configuration;

N_e, N_v = The molecular chain density of elastic chain and free chain;

$\widehat{\Phi}$, Φ = The strain energy of aging and unaged VEMs;

$\widehat{\Phi_f}$, Φ_f = The total strain energy of free chains of aging and unaged VEMs;

$\widehat{\Phi_e}$, Φ_e = The total strain energy of elastic chains of aging and unaged VEMs;

Φ_{e0}, Φ_{e1} = The strain energy of aging and unaged elastic chains;

κ = The aging function;

t_1, t_1^{ref} = The actual and reference aging time;

T, T_{ref} = The actual and reference aging temperature;

$\rho_{(\blacksquare)}$ = The influence function, in which （■） represents different reactions;

$E_{a,(\blacksquare)}$, $\delta_{(\blacksquare)}$ = The activation energy and the preexponential factor;

$A_{(\blacksquare)}$, $a_{T,(\blacksquare)}$ = The weight coefficient and the aging time-temperature shift factor;

Φ_{e1} = The strain energy of elastic chains formed from original elastic chains through SOC reaction;

P_f = The probability of forming a new crosslinking point on a single chain;

m_e = The average number of new formed crosslinking points on a single elastic chain;

m_f = The average number of new formed crosslinking points on a single free chain;

Φ_{e12} = The strain energy of elastic chains formed from original free chains through SOC reaction;

Φ_{f0}, Φ_{f1} = The strain energy of aging and unaged free chains;

P_s = The probability of losing a crosslinking point on a single elastic chain;

h = The average number of elastic chains connected to a crosslinking point;

Φ_{f1} = The strain energy of free chains generated from elastic chains;

Φ_{f12} = The strain energy of free chains formed from the original ones;

λ^{q_j}, χ^{q_j} = The microscopic tensile ratio and the macroscopic tensile ratio in direction q_j;

μ = The volume fraction of filler;

γ = The filler-reinforcement coefficient;

$\tilde{\mathbf{S}}$, $\mathbf{S}$ = The stress tensor of filler and unfilled system;

$\boldsymbol{F}$ = The deformation gradient;

p = An arbitrary scalar;

$\mathbf{C}$ = The right Cauchy green stress tensor.

Data availability statement

All data, models, and code generated or used during the study appear in the published article.

Acknowledgments

The authors acknowledge financial supports from the following funds: (1) National Key Research and Development Plans with Grant No. 2019YFE0121900; (2) The Jiangsu Province International Cooperation Project with Grant No. BZ2022037; (3) The Tencent Foundation through the XPLORER PRIZE; (4) The program of China Scholarships Council with Grant No. 202006090290; (5) National Natural Science Foundation of China with Grant No. 52208503.

References

[1] M. Uchida, K. Kamimura, T. Yoshida, Y. Kaneko, Viscoelastic-viscoplastic modeling of epoxy based on transient network theory, International Journal of Plasticity, 153 (2022) 103262.

[2] M. Shaafaey, A. Bahrololoumi, H. Mohammadi, S. Alazhary, R. Dargazany, Investigation of hygrothermal aging on the polyurethane-based (PUB) adhesive: substantiating competition scenario between sub-aging thermo-oxidation and hydrolytic phenomena, Journal of Polymer Research, 28 (2021) 1-25.

[3] Z.-D. Xu, T. Ge, J. Liu, Experimental and Theoretical Study of High-Energy Dissipation-Viscoelastic Dampers Based on Acrylate-Rubber Matrix, Journal of Engineering Mechanics, 146 (2020) 04020057.

[4] T. Ge, Z.-D. Xu, F.-G. Yuan, Development of Viscoelastic Damper Based on NBR and Organic Small-Molecule Composites, Journal of Materials in Civil Engineering, 34 (2022) 04022192.

[5] Z.-H. He, Z.-D. Xu, J.-Y. Xue, X.-J. Jing, Y.-R. Dong, Q.-Q. Li, Experimental study and mechanical model of viscoelastic damping limb-like-structure device with coupling nonlinear characteristics, Soil Dynamics and Earthquake Engineering, 160 (2022) 107385.

[6] Y.-R. Dong, Z.-D. Xu, Q.-Q. Li, Z.-H. He, X. Yan, Y. Cheng, Tests and Micro–Macro Cross-Scale Model of High-Performance Acrylate Viscoelastic Dampers Used in Structural Resistance, Journal of Structural Engineering, 149 (2023) 04023088.

[7] Y. Xu, Z.-D. Xu, Y.-Q. Guo, W. Sarwar, W. She, Z.-F. Geng, Study on viscoelastic materials at micro scale pondering supramolecular interaction impacts with DMA tests and fractional derivative modeling, Journal of Applied Polymer Science, 140 (2023) e53660.

[8] K.-C. Chang, Y.-Y. Lin, Seismic response of full-scale structure with added viscoelastic dampers, Journal of Structural Engineering, 130 (2004) 600-608.

[9] V. Kostarev, I. Tamura, M. Kuramasu, F. Barutzki, P. Vasilev, Y. Enomoto, Y. Namita, S. Okita, Y. Sato, Shaking Table Tests of a Piping System With Viscoelastic Dampers Subjected to Severe Earthquake Motions, in: Pressure Vessels and Piping Conference, American Society of Mechanical Engineers, 2016, pp. V008T008A005.

[10] Z.-D. Xu, P.-P. Gai, H.-Y. Zhao, X.-H. Huang, L.-Y. Lu, Experimental and theoretical study on a building structure controlled by multi-dimensional earthquake isolation and mitigation devices, Nonlinear Dynamics, 89 (2017) 723-740.

[11] Y.-R. Dong, Z.-D. Xu, Q. Shi, Q.-Q. Li, Z.-H. He, Y. Cheng, Seismic performance and material-level damage evolution of retrofitted RC framed structures by high-performance AVED under different shear-span ratio, Journal of Building Engineering, 63 (2023) 105495.

[12] R. Kadri, M.N. Abdelaziz, B. Fayolle, M.B. Hassine, J.F. Witz, A unified mechanical based approach to fracture properties estimates of rubbers subjected to aging, International Journal of Solids and Structures, 234-235 (2022) 111305.

[13] J. Yang, W. Lou, Molecule Dynamics Simulation of the Effect of Oxidative Aging on Properties of Nitrile Rubber, Polymers, 14 (2022) 226.

[14] A. Bahrololoumi, H. Mohammadi, V. Moravati, R. Dargazany, A Physically-Based Model for Thermo-Oxidative and Hydrolytic Aging of Elastomers, International Journal of Mechanical Sciences, 194 (2021).

[15] H. Mohammadi, V. Morovati, E. Poshtan, R. Dargazany, Understanding decay functions and their contribution in modeling of thermal-induced aging of cross-linked polymers, Polymer Degradation and Stability, 175 (2020) 109108.

[16] R. Han, Y. Wu, X. Quan, K. Niu, Effects of crosslinking densities on mechanical properties of nitrile rubber composites in thermal oxidative aging environment, Journal of Applied Polymer Science, 137 (2020) 49076.

[17] A. David, J. Huang, E. Richaud, P.Y. Le Gac, Impact of thermal oxidation on mechanical behavior of polydicylopentadiene: Case of non-diffusion limited oxidation, Polymer Degradation and Stability, 179 (2020) 109294.

[18] J. Zhi, Q. Wang, M. Zhang, Z. Zhou, A. Liu, Y. Jia, Coupled analysis on hyper-viscoelastic mechanical behavior and macromolecular network alteration of rubber during thermo-oxidative aging process, Polymer, 171 (2019) 15-24.

[19] G. Hamed, J. Zhao, Tensile behavior after oxidative aging of gum and black-filled vulcanizates of SBR and NR, Rubber chemistry and technology, 72 (1999) 721-730.

[20] T. Ishida, E. Richaud, M. Gervais, A. Gaudy, R. Kitagaki, H. Hagihara, Y. Elakneswaran, Thermal aging of acrylic-urethane network: Kinetic modeling and end-of-life criteria combined with mechanical properties, Progress in Organic Coatings, 163 (2022) 106654.

[21] B. Musil, M. Johlitz, A. Lion, On the ageing behaviour of NBR: chemomechanical experiments, modelling and simulation of tension set, Continuum Mechanics and Thermodynamics, 32 (2020) 369-385.

[22] S. Lejeunes, D. Eyheramendy, A. Boukamel, A. Delattre, S. Méo, K.D. Ahose, A constitutive multiphysics modeling for nearly incompressible dissipative materials: application to thermo–chemo-mechanical aging of rubbers, Mechanics of Time-Dependent Materials, 22 (2018) 51-66.

[23] A. Lion, M. Johlitz, On the representation of chemical ageing of rubber in continuum mechanics, International Journal of Solids and Structures, 49 (2012) 1227-1240.

[24] T. Ha-Anh, T. Vu-Khanh, Prediction of mechanical properties of polychloroprene during thermo-oxidative aging, Polymer Testing, 24 (2005) 775-780.

[25] W. Zheng, X. Zhao, Q. Li, T.W. Chan, L. Zhang, S. Wu, Compressive stress relaxation modeling of butadiene rubber under thermo‐oxidative aging, Journal of Applied Polymer Science, 134 (2017).

[26] J.Y. Zhi, Q.L. Wang, M.J. Zhang, M.J. Li, Y.X. Jia, Coupled analysis on heterogeneous oxidative aging and viscoelastic performance of rubber based on multi-scale simulation, Journal of Applied Polymer Science, 136 (2019) 47452.

[27] T. Zink, L. Kehrer, V. Hirschberg, M. Wilhelm, T. Böhlke, Nonlinear Schapery viscoelastic material model for thermoplastic polymers, Journal of Applied Polymer Science, n/a 52028.

[28] H. Mohammadi, V. Morovati, A.-E. Korayem, E. Poshtan, R. Dargazany, Constitutive Modeling of Elastomers During Photo- and Thermo-oxidative Aging, Polymer Degradation and Stability, 191 (2021) 109663.

[29] A. Bahrololoumi, V. Morovati, E.A. Poshtan, R. Dargazany, A multi-physics constitutive model to predict hydrolytic aging in quasi-static behaviour of thin cross-linked polymers, International Journal of Plasticity, 130 (2020) 102676.

[30] Tang, Shan, S. Greene, Liu, W. Kam, Two-scale mechanism-based theory of nonlinear viscoelasticity, Journal of the Mechanics and Physics of Solids, 60 (2012) 199-226.

[31] J. Fröhlich, W. Niedermeier, H.D. Luginsland, The effect of filler–filler and filler–elastomer interaction on rubber reinforcement, Composites Part A: Applied Science and Manufacturing, 36 (2005) 449-460.

[32] J. Wang, H. Jia, L. Ding, X. Xiong, X. Gong, The mechanism of carbon–silica dual phase filler modified by ionic liquid and its reinforcing on natural rubber, Polymer Composites, 36 (2015) 1721-1730.

[33] A.R. Payne, The dynamic properties of carbon black‐loaded natural rubber vulcanizates. Part I, Journal of applied polymer science, 6 (1962) 57-63.

[34] Q.-Q. Li, Z.-D. Xu, Y.-R. Dong, Z.-H. He, J.-X. He, Y. Lu, Microstructure-Based Equivalent Visco-Hyperelastic Model of Viscoelastic Damper, Journal of Engineering Mechanics, 148 (2022) 04022014.

[35] Y. Xu, Z.-D. Xu, Y.-Q. Guo, Y. Dong, T. Ge, C. Xu, Tests and Modeling of Viscoelastic Damper Considering Microstructures and Displacement Amplitude Influence, Journal of Engineering Mechanics, 145 (2019) 04019108.

[36] R. Bouaziz, K. Ahose, S. Lejeunes, D. Eyheramendy, F. Sosson, Characterization and modeling of filled rubber submitted to thermal aging, International Journal of Solids and Structures, 169 (2019) 122-140.

[37] N. Rezig, T. Bellahcene, M. Aberkane, M.N. Abdelaziz, Thermo-oxidative ageing of a SBR rubber: effects on mechanical and chemical properties, Journal of Polymer Research, 27 (2020) 1-13.

[38] R. Bouaziz, K.D. Ahose, S. Lejeunes, D. Eyheramendy, F. Sosson, Characterization and modeling of filled rubber submitted to thermal aging, International Journal of Solids and Structures, 169 (2019) 122-140.

[39] S. He, F. Bai, S. Liu, H. Ma, J. Hu, L. Chen, J. Lin, G. Wei, X. Du, Aging properties of styrene-butadiene rubber nanocomposites filled with carbon black and rectorite, Polymer Testing, 64 (2017) 92-100.

[40] M. Nait Abdelaziz, G. Ayoub, X. Colin, M. Benhassine, M. Mouwakeh, New developments in fracture of rubbers: Predictive tools and influence of thermal aging, International Journal of Solids and Structures, 165 (2019) 127-136.

[41] A. Najmeddine, Z. Xu, G. Liu, Z.L. Croft, G. Liu, A.R. Esker, M. Shakiba, Physics and chemistry-based constitutive modeling of photo-oxidative aging in semi-crystalline polymers, International Journal of Solids and Structures, (2022) 111427.

[42] V. Morovati, M.A. Saadat, R. Dargazany, Necking of double-network gels: Constitutive modeling with microstructural insight, Physical Review E, 102 (2020) 062501.

[43] S. Konica, T. Sain, A thermodynamically consistent chemo-mechanically coupled large deformation model for polymer oxidation, Journal of the Mechanics and Physics of Solids, 137 (2020) 103858.

[44] P.D. Wu, E. Giessen, On improved network models for rubber elasticity and their applications to orientation hardening in glassy polymers, Journal of the Mechanics & Physics of Solids, 41 (1993) 427-456.

[45] P. Bažant, B. Oh, Efficient numerical integration on the surface of a sphere, ZAMM ‐ Journal of Applied Mathematics and Mechanics/Zeitschrift für Angewandte Mathematik und Mechanik, 66 (1986) 37-49.

[46] V. Morovati, R. Dargazany, An improved non-gaussian statistical theory of rubber elasticity for short chains, in: ASME 2018 International Mechanical Engineering Congress and Exposition, American Society of Mechanical Engineers Digital Collection, 2018.

[47] V. Morovati, H. Mohammadi, R. Dargazany, A generalized approach to generate optimized approximations of the inverse Langevin function, Mathematics and Mechanics of Solids, 24 (2019) 2047-2059.

[48] R. Dargazany, V.N. Khiêm, U. Navrath, M. Itskov, Network evolution model of anisotropic stress softening in filled rubber-like materials: Parameter identification and finite element implementation, Journal of Mechanics of Materials and Structures, 7 (2013) 861-885.

[49] H. Dal, C. Zopf, M. Kaliske, Micro-sphere based viscoplastic constitutive model for uncured green rubber, International Journal of Solids and Structures, 132-133 (2018) 201-217.

[50] M. Hossain, G. Possart, P. Steinmann, A finite strain framework for the simulation of polymer curing. Part I: elasticity, Computational Mechanics, 44 (2009) 621-630.

[51] Q.-Q. Li, Z.-D. Xu, Y.-R. Dong, Z.-H. He, J.-X. He, X. Yan, Hyperelastic Hybrid Molecular Chain Model of Thermal-Oxidative Aging Viscoelastic Damping Materials Based on Physical–Chemical Process, Journal of Engineering Mechanics, 149 (2023) 04022099.